Published OnlineFirst February 24, 2020; DOI: 10.1158/0008-5472.CAN-19-2714

FGF Trapping Inhibits Multiple Myeloma Growth through c-Myc Degradation–Induced Mitochondrial Oxidative Stress

Roberto Ronca[1], Gaia C. Ghedini[1], Federica Maccarinelli[1], Antonio Sacco[2], Silvia L. Locatelli[3], Eleonora Foglio[1], Sara Taranto[1], Elisabetta Grillo[1], Sara Matarazzo[1], Riccardo Castelli[4], Giuseppe Paganini[1], Vanessa Desantis[5], Nadia Cattane[6], Annamaria Cattaneo[6,7], Marco Mor[4], Carmelo Carlo-Stella[3], Angelo Belotti[8], Aldo M. Roccaro[2], Marco Presta[1], and Arianna Giacomini[1]

ABSTRACT

Multiple myeloma, the second most common hematologic malignancy, frequently relapses because of chemotherapeutic resistance. Fibroblast growth factors (FGF) act as proangiogenic and mitogenic cytokines in multiple myeloma. Here, we demonstrate that the autocrine FGF/FGFR axis is essential for multiple myeloma cell survival and progression by protecting multiple myeloma cells from oxidative stress–induced apoptosis. In keeping with the hypothesis that the intracellular redox status can be a target for cancer therapy, FGF/FGFR blockade by FGF trapping or tyrosine kinase inhibitor impaired the growth and dissemination of multiple myeloma cells by inducing mitochondrial oxidative stress, DNA damage, and apoptotic cell death that were prevented by the antioxidant vitamin E or mitochondrial catalase overexpression. In addition, mitochondrial oxidative stress occurred as a consequence of proteasomal degradation of the c-Myc oncoprotein that led to glutathione depletion. Accordingly, expression of a proteasome-nondegradable c-Myc protein mutant was sufficient to avoid glutathione depletion and rescue the proapoptotic effects due to FGF blockade. These findings were confirmed on bortezomib-resistant multiple myeloma cells as well as on bone marrow–derived primary multiple myeloma cells from newly diagnosed and relapsed/refractory patients, including plasma cells bearing the t(4;14) translocation obtained from patients with high-risk multiple myeloma. Altogether, these findings dissect the mechanism by which the FGF/FGFR system plays a nonredundant role in multiple myeloma cell survival and disease progression, and indicate that FGF targeting may represent a therapeutic approach for patients with multiple myeloma with poor prognosis and advanced disease stage.

Significance: This study provides new insights into the mechanisms by which FGF antagonists promote multiple myeloma cell death.

Graphical Abstract: http://cancerres.aacrjournals.org/content/canres/80/11/2340/F1.large.jpg.

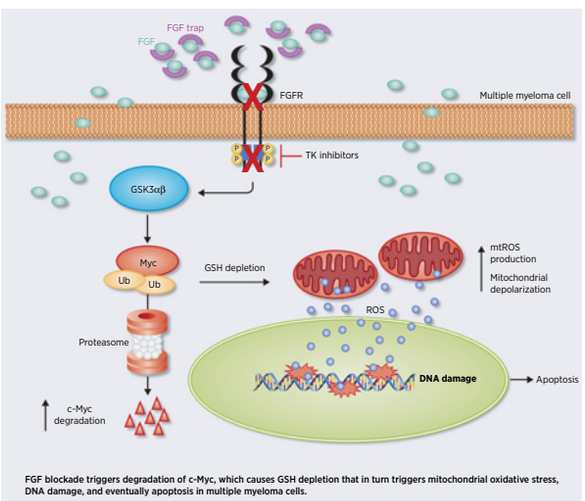

FGF blockade triggers degradation of c-Myc, which causes GSH depletion that in turn triggers mitochondrial oxidative stress, DNA damage, and eventually apoptosis in multiple myeloma cells.

Introduction

Multiple myeloma represents the second most common hematologic malignancy (1) and is characterized by the clonal proliferation of malignant plasma cells within the bone marrow (BM; ref. 2). Multiple myeloma relapses in the majority of patients because of chemotherapeutic resistance, indicating that novel biologically based treatments are urgently required.

Multiple myeloma cells' behavior is determined by their genetic background and cross-talk with the BM microenvironment that activates a pleiotropic cascade of proliferative/antiapoptotic signaling

[1]Department of Molecular and Translational Medicine, University of Brescia, Brescia, Italy. [2]Clinical Research Development and Phase I Unit, CREA Laboratory, ASST Spedali Civili di Brescia, Brescia, Italy. [3]Department of Oncology and Hematology, Humanitas Clinical and Research Center - IRCCS and Humanitas University, Milan, Italy. [4]Department of Food and Drug, University of Parma, Parma, Italy. [5]Department of Biomedical Sciences and Human Oncology, Azienda Ospedaliera Consorziale Universitaria Policlinico di Bari, Bari, Italy. [6]Biological Psychiatry Unit, IRCCS Istituto Centro San Giovanni di Dio Fatebenefratelli, Brescia, Italy. [7]Stress, Psychiatry and Immunology Laboratory, Department of Psychological Medicine, Institute of Psychiatry, King's College London, London, United Kingdom. [8]Department of Hematology, ASST Spedali Civili di Brescia, Brescia, Italy.

Note: Supplementary data for this article are available at Cancer Research Online (http://cancerres.aacrjournals.org/).

Corresponding Authors: Arianna Giacomini, University of Brescia, Viale Europa 11, Brescia 25123, Italy. Phone: 3903-0371-7734; Fax: 3903-0371-7747; E-mail: arianna.giacomini@unibs.it; and Marco Presta, marco.presta@unibs.it

Cancer Res 2020;80:2340–54

doi: 10.1158/0008-5472.CAN-19-2714

Published OnlineFirst February 24, 2020; DOI: 10.1158/0008-5472.CAN-19-2714

pathways (3, 4). These events are triggered by the production of several growth factors by BM stromal cells (BMSC) and/or multiple myeloma cells in a paracrine/autocrine manner, leading to disease progression and drug resistance. In this frame, fibroblast growth factors (FGF) play a pivotal role acting as potent proangiogenic mediators (5, 6) and mitogenic cytokines (7–9). Elevated levels of FGF2 are detectable in the BM and serum of patients with multiple myeloma and correlate with disease activity (10, 11). In addition, patient-derived multiple myeloma cells secrete FGF2, representing the prevailing source in the BM of patients with active disease (7).

The relevance of autocrine/paracrine FGF signaling in multiple myeloma is supported by the observation that FGF receptors (FGFR) are expressed by multiple myeloma cell lines, patient-derived multiple myeloma cells, and within the BM milieu (7, 9, 12). Also, FGFR3 has been implicated in multiple myeloma cell proliferation and survival (13–15) and 15% of patients with multiple myeloma overexpress FGFR3 due to a t(4;14)(p16.3;q32) translocation (16). Although a small fraction of these patients harbor a FGFR3-activating mutation, the majority of them upregulate the wild-type FGFR3 receptor, thus depending on FGF ligand for activation (17). Multiple myeloma cells express various FGFs, including FGF2, regardless of FGFR3 upregulation (9, 18), suggesting that autocrine FGF signaling may contribute to multiple myeloma growth also independently from deregulated FGFR expression.

Altogether, these findings make the FGF/FGFR system a promising target in multiple myeloma therapy, and FGF inhibitors may exert a simultaneous "two compartment" effect by hampering autocrine/paracrine oncogenic signaling in multiple myeloma (19). Accordingly, clinical trials are in progress to assess the effect of the inhibition of the FGF signaling by selective tyrosine kinase (TK) FGFR inhibitors in multiple myeloma (ClinicalTrials.gov). Recently, we have identified the PTX3-derived small-molecule NSC12 as the first orally active pan-FGF trap able to inhibit FGFR activation and tumor growth in various FGF-dependent murine and human cancer models (20, 21). Notably, extracellular FGF traps, including NSC12, appear to be devoid of the toxicities associated to TK FGFR inhibitors (21, 22), thus representing a potential alternative to inhibit the FGF/FGFR system in multiple myeloma.

Here, we dissected for the first time the mechanism by which the FGF/FGFR system plays a nonredundant role in multiple myeloma cell survival and disease progression. Our findings reveal that blockade of FGF/FGFR signaling by NSC12 or selective TK FGFR inhibitor triggers mitochondrial oxidative stress, DNA damage and apoptotic cell death via the proteasomal degradation of the c-Myc oncoprotein in multiple myeloma cell lines and patient-derived multiple myeloma cells, including bortezomib-resistant multiple myeloma cells and tumor cells isolated from relapsed/refractory multiple myeloma patients. Together, our data provide novel information about the use of FGF/FGFR inhibitors in patients with relapsed/refractory multiple myeloma and raise possible concerns about their combination with proteasome inhibitors in clinical setting for multiple myeloma treatment.

Materials and Methods

Cell cultures and reagents

KMS-11 and KMS-11/BTZ cells were obtained from the Japanese Collection of Research Bioresources (JCRB) cell bank; RPMI8226, U-266, and OPM-2 cells from the German Collection of Microorganisms and Cell Cultures (DSMZ); MM.1S cells from ATCC; GFP/Luciferase-expressing MM.1S cells were from Dr. Ghobrial, (Dana-Farber Cancer Institute, Boston, MA). All cell lines were maintained at low passage in RPMI1640 medium supplemented with 10% heat-inactivated FBS and 2.0 mmol/L glutamine, tested regularly for *Mycoplasma* negativity, and authenticated by PowerPlex Fusion System (Promega).

For lentiviral transduction of KMS-11 cells, particles coding for the mitochondrial catalase (pLVX-EF1a-IRES-puro-CatalaseMito; ref. 23), the cytoplasmic catalase (pLVX-IRES-neo-hCatalaseCito; ref. 23), or the mutated Myc (Lenti-Myc T58A, Gentaur s.r.l) were used.

For details about the reagents used, see the reagent table in Supplementary Information.

Cytofluorimetric analyses

Cytofluorimetric analyses were performed using the MACSQuant Analyzer (Miltenyi Biotec). Viable cell counting and cell-cycle analyses were performed as described in ref. 21. Mitochondrial membrane depolarization, mitochondrial (mt)ROS production and glutathione (GSH) levels were determined using the fluorescent probes tetramethylrhodamine ethyl ester, Mitosox, and Thiol-Tracker Violet (Thermo Fischer Scientific), respectively. Apoptotic cell death was assessed by Annexin-V/Propidium Iodide double staining (Immunostep) according to manufacturer's instructions.

Western blot analysis

Cells were washed in cold PBS and homogenized in NP-40 lysis buffer (1% NP-40, 20 mmol/L Tris-HCl pH 8, 137 mmol/L NaCl, 10% glycerol, 2 mmol/L EDTA, 1 mmol/L sodium orthovanadate, 10 μg/mL aprotinin, 10 μg/mL leupeptin). Protein concentration in the supernatants was determined using the Bradford protein assay (Bio-Rad Laboratories). Activation of signaling pathways and expression of specific proteins were detected using specific antibodies indicated in the reagent table in Supplementary Information.

For murine BM analysis, femurs were explanted from mice systemically injected with GFP/Luciferase-expressing MM.1S cells, flushed using PBS, and cells collected and processed as indicated above. β-Actin, α-tubulin, or GAPDH were used as loading controls (see reagent table in Supplementary Information for antibodies details). Chemiluminescent signal was acquired by ChemiDoc Imaging System (Bio-Rad) and analyzed using the ImageJ software (http://rsb.info.nih.gov/ij/).

Multiple myeloma/BMS cells' cocultures

KMS-11 cells were cocultured with patient-derived BMS cells at 15:1 multiple myeloma/BMSCs ratio. After 24 hours, NSC12 6.0 μmol/L was added to the cocultures. Forty-eight hours after treatment, KMS-11 cells were harvested without detaching BMS cells and KMS-11 viable cell counting was performed by cytofluorimetric analysis.

Chemotaxis assay

To evaluate MM.1S cell migration *in vitro*, cells were treated with 1.0 and 3.0 μmol/L NSC12 for 3 hours. Then, the cells were washed and seeded in the top compartment of a Boyden chamber containing gelatin-coated PVP-free polycarbonate filters (8-μm pore size). RPMI medium supplemented with 10% FBS or 50 ng/mL SDF1α was placed in the bottom compartment. After 12 hours of incubation at 37°C, cells that migrated to the bottom side of the filter were stained with Di-Quik reagent. Five random fields were counted for each triplicate sample.

Human phospho-protein proteome profiler array

Lysates (200 μg) from DMSO- and NSC12-treated cells were incubated with the Human Phospho-Kinase array Kit (R&D Systems)

Published OnlineFirst February 24, 2020; DOI: 10.1158/0008-5472.CAN-19-2714

according to manufacturer's instructions. Chemiluminescent signal was acquired and analyzed using the ImageJ software.

Genome-wide expression profiling

Genome-wide expression profiling (GEP) was performed on cells treated with NSC12 (6 μmol/L) for 6 or 12 hours, as reported in Supplementary Information. A cut-off of $P < 0.01$ (FDR corrected) and $\log_2$ fold change $\pm$ 2 was applied to select differentially expressed genes.

RT-PCR and qRT-PCR

Total RNA was extracted using TRIzol Reagent (Invitrogen) according to manufacturer's instructions. Two micrograms of total RNA were retrotranscribed with MMLV reverse transcriptase (Invitrogen) using random hexaprimers. Then, cDNA was analyzed by semiquantitative or quantitative PCR using primers indicated in the reagent table in Supplementary Information.

Seahorse analysis

KMS-11 cells were seeded at 4×10^5 cells/well on Seahorse XFe24 culture plates (Agilent) previously treated with 3.5 μg/cm^2 Corning Cell-Tak Cell and Tissue Adhesive. Oxygen consumption rate (OCR) and extracellular acidification rate measurements were performed using a Seahorse XFe24 Extracellular Flux Analyzer (XFe Wave software). For further details, see Supplementary Information.

Subcutaneous human xenografts

Experiments were performed according to the Italian laws (D.L. 116/92 and following additions) that enforce the EU 86/109 Directive and were approved by the local animal ethics committee (OPBA, Organismo Preposto al Benessere degli Animali, Università degli Studi di Brescia, Italy).

Six- to 8-week-old female NOD/SCID mice (Envigo) were injected subcutaneously with KMS-11, RPMI8226 or KMS-11 cells overexpressing cytoplasmic or mitochondrial catalase (5×10^6 cells/mouse) in 200 μL of PBS. When tumors were palpable, mice were randomly assigned to receive treatment with NSC12 (7.5 mg/kg), vitamin E (150 mg/kg), or control/vehicle DMSO. Treatments were performed by oral gavage [DMSO/water (1:1)] in 100 μL final volume or intraperitoneally. Tumor volumes were measured with caliper and calculated according to the formula $V = (D \times d^2)/2$, where D and d are the major and minor perpendicular tumor diameters, respectively. At the end of the experimental procedure, tumor nodules were excised and processed for histologic analysis.

For alginate implant assay, mice were injected subcutaneously with 450 μL of 3% (w/v) sodium alginate solution (alginic acid dissolved in lipopolysaccharide -free PBS) containing 5×10^6 KMS-11 cells. After 7 days, mice received oral daily treatment with NSC12 (7.5 mg/kg) for 4 days. Alginate plugs were then harvested and processed for Western blot and histologic analyses.

Systemic human xenografts

Experiments were performed according to the Italian laws (D.L. 116/92 and following additions) that enforce the EU 86/109 Directive and were approved by the local animal ethics committee (OPBA, Organismo Preposto al Benessere degli Animali, Università degli Studi di Brescia, Italy).

Six- to 8-week-old female SCID Beige mice (Envigo) were injected intravenously with GFP/Luciferase-expressing MM.1S cells (2×10^6 cells/mouse) in 100 μL of PBS. Mice were randomly assigned to receive short- or long-term intraperitoneal treatments with NSC12 (7.5 mg/kg) or control/vehicle DMSO. For further details, see Supplementary Information.

Cytologic and histologic analyses

Cytospin from patient-derived multiple myeloma cells were prepared using about 2×10^5 cells/slide. Tumor samples were either embedded in OCT compound and immediately frozen or fixed in formalin and embedded in paraffin. All samples were further processed as reported in Supplementary Information.

Zebrafish embryo homing model

The model was used as described in ref. 24. Briefly, MM.1S cells were exposed for 3 hours to NSC12 3 μmol/L or DMSO. Thirty minutes before the end of treatment, CMTPX or CMF2HC CellTracker dyes (Thermo Fisher Scientific) were added to cell suspensions to obtain fluorescently labeled red (NSC12-treated) or blue (DMSO-treated) MM.1S cells, respectively. After staining, NSC12- and DMSO-treated cells were washed, mixed together at a 1:1 ratio, and coinjected in the bloodstream of zebrafish embryos by the duct of Cuvier. Zebrafish experiments were performed as approved by the local animal ethics committee (OPBA, Organismo Preposto al Benessere degli Animali, Università degli Studi di Brescia, Italy). For further details, see Supplementary Information.

Patient-derived multiple myeloma cells

This study was approved by the Institutional Review Board at Humanitas Cancer Center of Rozzano (Milan) and conducted in accordance with GCP and the Declaration of Helsinki. Written informed consent was obtained from all patients. Primary CD138$^+$ cells were obtained from freshly isolated multiple myeloma patients' BM using CD138$^+$ microbeads selection, as reported in ref. 25.

Statistical analyses

Statistical analyses were performed using Prism 6 (GraphPad Software). Student t test for unpaired data (two-tailed) was used to test the probability of significant differences between two groups of samples. For more than two groups of samples, data were analyzed with a one-way ANOVA and corrected by the Bonferroni multiple comparison test. Tumor volume data were analyzed with a two-way ANOVA and corrected by the Bonferroni test. Differences were considered significant when $P < 0.05$ unless otherwise specified.

Code and data availability

For original data, please contact arianna.giacomini@unibs.it. Microarray data are available at GEO under accession number GSE129279.

Results

Inhibition of FGF/FGFR signaling triggers apoptosis of multiple myeloma cells

A FGF autocrine/paracrine loop of stimulation has been described in multiple myeloma (7, 26, 27). Accordingly, the human multiple myeloma cell lines harboring (KMS-11 and OPM-2 cells) or not (RPMI8226 and U-266 cells) the t(4;14) translocation express different FGFs and FGFRs (Supplementary Fig. S1A). Autocrine activation of the FGF/FGFR system in these cells was confirmed by FGFR/FRS2 phosphorylation that occurs in the absence of exogenous stimuli (Supplementary Fig. S1A). On this basis, to assess the impact exerted by the inhibition of this autocrine FGF/FGFR axis on multiple

Published OnlineFirst February 24, 2020; DOI: 10.1158/0008-5472.CAN-19-2714

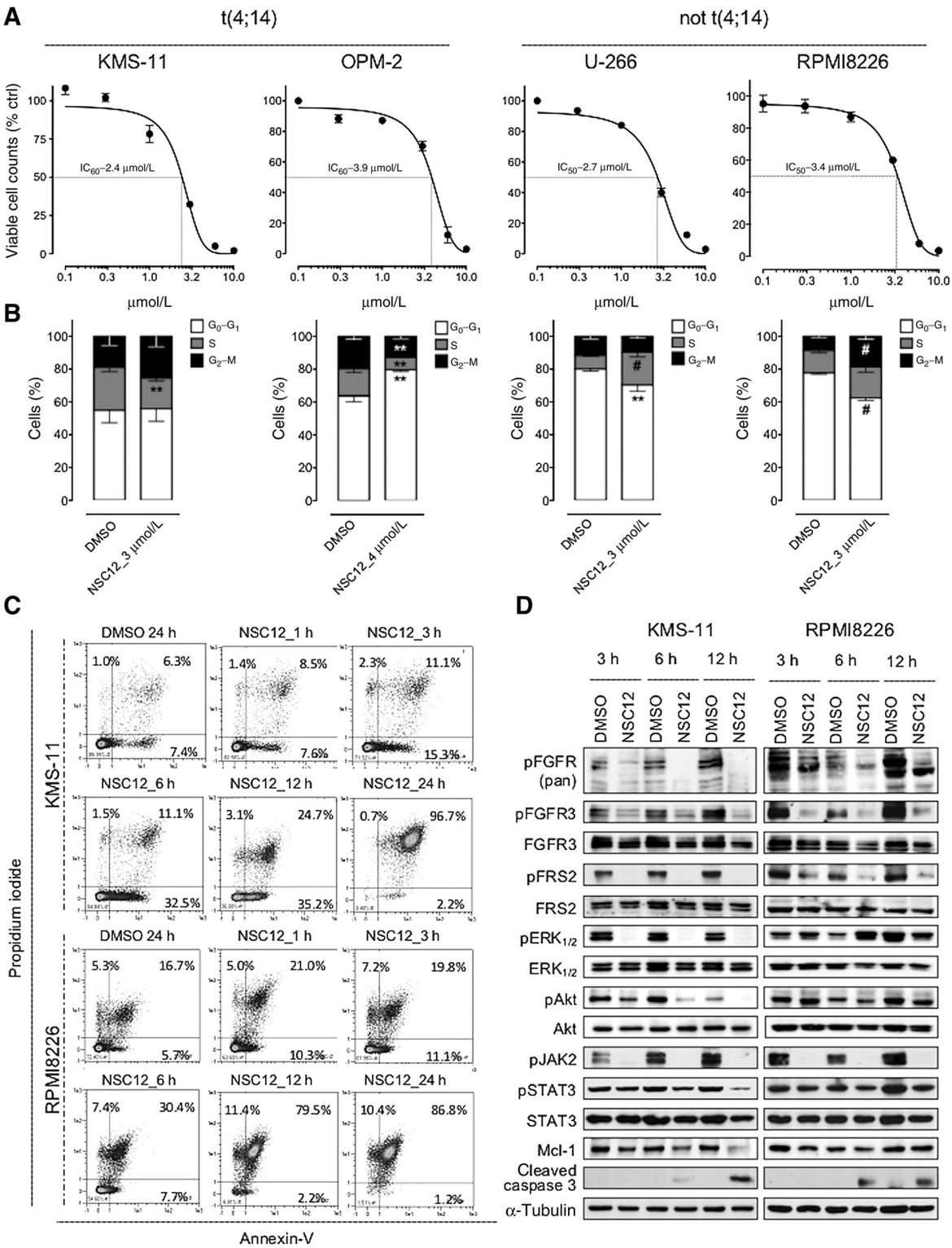

Figure 1.

In vitro effects of FGF blockade in MM cells. **A,** Viable cell counts by cytofluorimetric analysis of MM cell lines harboring or not the t(4;14) and treated with NSC12 for 72 hours. Data are mean ± SEM. **B,** Cell-cycle analysis of multiple myeloma cell lines harboring or not the t(4;14) and treated with NSC12 for 72 hours. Data are mean ± SEM. **, $P < 0.01$; #, $P < 0.001$. **C,** Cytofluorimetric analysis of apoptotic cell death of t(4;14)-positive KMS-11 and t(4;14)-negative RPMI8226 cells after treatment with NSC12 6 μmol/L. **D,** Western blot analysis of KMS-11 and RPMI8226 cells after treatment with NSC12 6 μmol/L.

Published OnlineFirst February 24, 2020; DOI: 10.1158/0008-5472.CAN-19-2714

myeloma cell proliferation/survival, the four cell lines were treated with increasing doses of the pan-FGF trap molecule NSC12 (20, 21). When treated with NSC12, t(4;14)-positive and t(4;14)-negative multiple myeloma cells showed impaired cell proliferation and survival, with alterations of cell cycle (**Fig. 1A** and **B**). Cell-cycle analysis revealed a significant reduction of the S-phase in KMS-11 and OPM-2 cells, whereas an accumulation in the S- and G_2–M-phase was observed in RPMI8226 and U-266 cells, respectively (**Fig. 1B**). Both KMS-11 and RPMI8226 cells showed a significant increase of apoptotic cells 6 hours after NSC12 treatment with 100% cell death at 24 hours (**Fig. 1C**; Supplementary Fig. S1B).

The specificity of NSC12 on the blockade of FGF/FGFR system has been previously reported (21). To corroborate these evidences also in multiple myeloma models, we performed rescue experiments by adding exogenous recombinant FGF2 to KMS-11 cell cultures treated with NSC12 3 μmol/L and assessing cell death 48 hours after treatment. An excess of exogenous FGF2 significantly reduced KMS-11 cell death induced by NSC12, thus confirming the specificity of the compound (Supplementary Fig. S1C). Accordingly, NSC12 inhibited FGFR phosphorylation, activation of MAPK, Akt and JAK/STAT3 pathways, leading to the activation of caspase-3 in both cell lines (**Fig. 1D**). Similar results were obtained after treatment with the TK FGFR inhibitor BGJ398 (Supplementary Fig. S1D–S1F).

Mcl-1 is an important survival factor for multiple myeloma cells (28) and the activation of the FGF/FGFR system can promote *MCL-1* expression via the activation of the transcription factors NF-κB and STAT3 (29). Accordingly, NSC12 treatment reduced mcl-1 protein levels in KMS-11 and RPMI8226 cells, even though with different kinetics. Indeed, mcl-1 protein levels resulted significantly reduced at each time point in NSC12-treated KMS-11 cells, whereas no significant changes were detected in RPMI8226 cells after 6 and 12 hours of treatment with NSC12 (**Fig. 1D**) despite the strong increase in apoptotic cells observed at these time points (**Fig. 1C**). These data suggest that mcl-1 downmodulation does not represent a major mechanism leading to multiple myeloma cell death upon FGF/FGFR inhibition.

Notably, a significant reduction of multiple myeloma cell survival was observed also when KMS-11 cells were cocultured with patient-derived BMSCs and treated with NSC12, suggesting that FGF trapping might disrupt FGF-mediated BMSC/multiple myeloma cell cross-talk (Supplementary Fig. S1G and S1H).

In keeping with the *in vitro* observations, oral treatment with NSC12 caused a significant inhibition of FGFR3 phosphorylation (**Fig. 2A**) and tumor growth when KMS-11 and RPMI8226 cells were grafted subcutaneously in immunodeficient mice (**Fig. 2B**). This was accompanied by inhibition of tumor cell proliferation and increased apoptosis, as revealed by phospho-Histone H3 and TUNEL immunostaining, respectively (**Fig. 2C**). In keeping with the role of the FGF/FGFR system in tumor angiogenesis, NSC12-treated tumors showed also a decrease in $CD31^+$ vascularization (Supplementary Fig. S1H).

FGF trapping inhibits multiple myeloma dissemination

The MM.1S cell line represents an experimental platform suitable for the study of multiple myeloma dissemination *in vivo* (30, 31). MM.1S cells express all four FGFRs and FGF2/3/9 (Supplementary Fig. S1A). NSC12 administration hampered FGFR1 and FGFR3 phosphorylation also in these cells (**Fig. 3A**; Supplementary Fig. S1J), thus inhibiting their proliferation and increasing the number of apoptotic cells at 6 hours after treatment (**Fig. 3B**). Notably, NSC12-treated cells were characterized by a decreased capacity to migrate toward chemotactic stimuli represented by FBS or the SDF1α chemokine (**Fig. 3C**). FAK kinase and β-catenin are regulated by FGF/FGFR signaling (32–34) and support the migration and adhesion of multiple myeloma cells in the BM niche (35, 36). Accordingly, NSC12 strongly reduced FAK phosphorylation and the levels of FAK and β-catenin in MM.1S cells (**Fig. 3D**), indicating a link between the FGF/FGFR axis and multiple myeloma cell migration.

To investigate whether NSC12 might affect the homing of multiple myeloma cells to the BM, we took advantage of a zebrafish embryo model in which the caudal hematopoietic tissue (CHT) recapitulates a BM-like niche (24). MM.1S cells were stained with a red or blue fluorescent dye and treated with vehicle (DMSO) or NSC12, respectively. After 3 hours, an incubation time that does not cause MM.1S cell death, the two cell preparations were mixed together (1:1 ratio) and coinjected in the bloodstream of zebrafish embryos (**Fig. 3E**). As shown in **Fig. 3F**, NSC12 pretreatment significantly prevented multiple myeloma cell homing to the CHT when compared with DMSO-treated cells.

Next, GFP/Luciferase-expressing MM.1S cells were systemically injected in SCID beige mice. BM infiltration was detectable 2 weeks after injection and reached a peak after 6–8 weeks, when approximately 40% of the BM cell population was represented by tumor cells (**Fig. 3G**). On this basis, mice bearing 10%–20% of MM.1S cell BM colonization/infiltration were treated for 3 days with NSC12. BM analysis showed that NSC12 reduced the levels of phosphorylated FGFR3 in NSC12-treated mice to those detected in disease-free animals (**Fig. 3H**). Accordingly, chronic NSC12 treatment significantly reduced BM tumor burden in MM.1S cell–grafted animals (**Fig. 3I**). Together, these data indicate that NSC12 inhibits FGF/FGFR signaling and proliferation of multiple myeloma cells growing within their own microenvironment.

Inhibition of FGF signaling induces oxidative stress–mediated DNA damage and apoptosis in multiple myeloma cells

To get further insights into the impact of FGF inhibition in multiple myeloma, GEP analysis was performed on NSC12-treated KMS-11 cells. The analysis revealed a significant $\log_2$ 2-fold upregulation of 33 and 44 genes after 6 and 12 hours of treatment, respectively (**Fig. 4A**; Supplementary Fig. S2A), the majority of them being related to oxidative stress and DNA damage (Supplementary Table S1; Supplementary Fig. S2B). Accordingly, phospho-kinase array analysis showed the activation of oxidative stress- and DNA damage–induced protein kinases and confirmed the inactivation of Akt, Erk, and STAT kinases as well as reduced levels of FAK and β-catenin phosphorylation (Supplementary Fig. S2C). Together, these data suggest that the autocrine FGF/FGFR axis may play a role in preventing oxidative stress and consequent DNA damage in multiple myeloma cells.

In keeping with this hypothesis, NSC12 rapidly increased mtROS production and mitochondrial membrane depolarization in KMS-11 (**Fig. 4B**) and RPMI8226 (Supplementary Fig. S2D) cells. mtROS production was paralleled by PARP inactivation and extensive DNA damage, as assessed by increased levels of phospho-H2AX (γH2AX; **Fig. 4C**). Accordingly, NSC12 caused a strong reduction of mitochondrial respiration 1 hour after treatment and a complete dysfunction of mitochondrial activity 3 hours thereafter, leading to mitochondrial proton leak and medium acidification (**Fig. 4D**; Supplementary Fig. S2E). Notably, NSC12 treatment did not cause the reduction of the oxidative stress–protective transcription factor Nrf2, which resulted instead slightly increased 12 hours after treatment with the compound (Supplementary Fig. S2F), suggesting Nfr2 is not

Published OnlineFirst February 24, 2020; DOI: 10.1158/0008-5472.CAN-19-2714

implicated in the mitochondrial oxidative stress induced by FGF inhibition. However, the activation of Nrf2 that occurs 12 hours after NSC12 treatment may represent a downstream effect by which the cells try to compensate the oxidative stress status caused by FGF inhibition.

Oxidative stress and DNA damage were observed also in tumor xenografts treated with NSC12, as assessed by anti-nitro tyrosine and anti-pH2AX staining, respectively (**Fig. 4E**). Notably, administration of the antioxidant vitamin E prevented NSC12-induced mtROS production, mitochondrial depolarization, DNA damage, and apo-

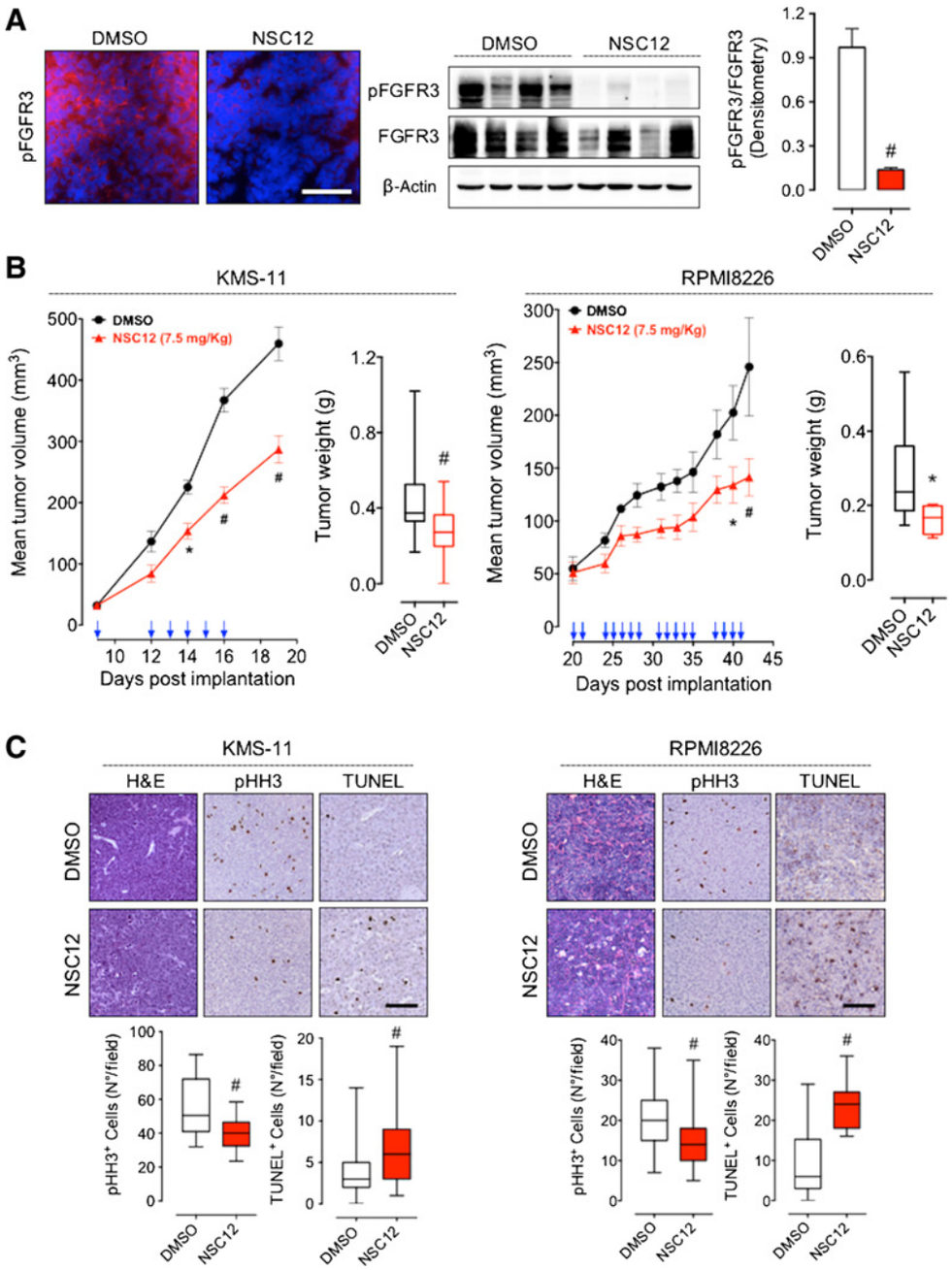

Figure 2.

FGF trapping inhibits multiple myeloma growth *in vivo*. **A,** Analysis of phospho-FGFR3 levels by immunofluorescence (left) and Western blot (right) in subcutaneous KMS-11 alginate plugs after 4-day oral treatment with NSC12 7.5 mg/kg ($n = 4$ mice/group). pFGFR3/FGFR3 densitometry was quantified with ImageJ software and normalized to β-actin. Scale bar, 100 μm. **B,** Tumor growth of KMS-11 and RPMI8226 cells injected subcutaneously and orally treated (arrows) with NSC12 or vehicle ($n = 10$ mice/group). **C,** IHC analysis of KMS-11 and RPMI8226 tumors harvested at the end of the experiment described in **B**. Quantification of pHH3- and TUNEL-positive cells was carried out by ImageJ software. Scale bar, 50 μm. Data are mean ± SEM. In box and whisker graphs, boxes extend from the 25th to the 75th percentiles, lines indicate the median values, and whiskers indicate the range of values. *, $P < 0.05$; #, $P < 0.001$. H&E, hematoxylin and eosin.

Published OnlineFirst February 24, 2020; DOI: 10.1158/0008-5472.CAN-19-2714

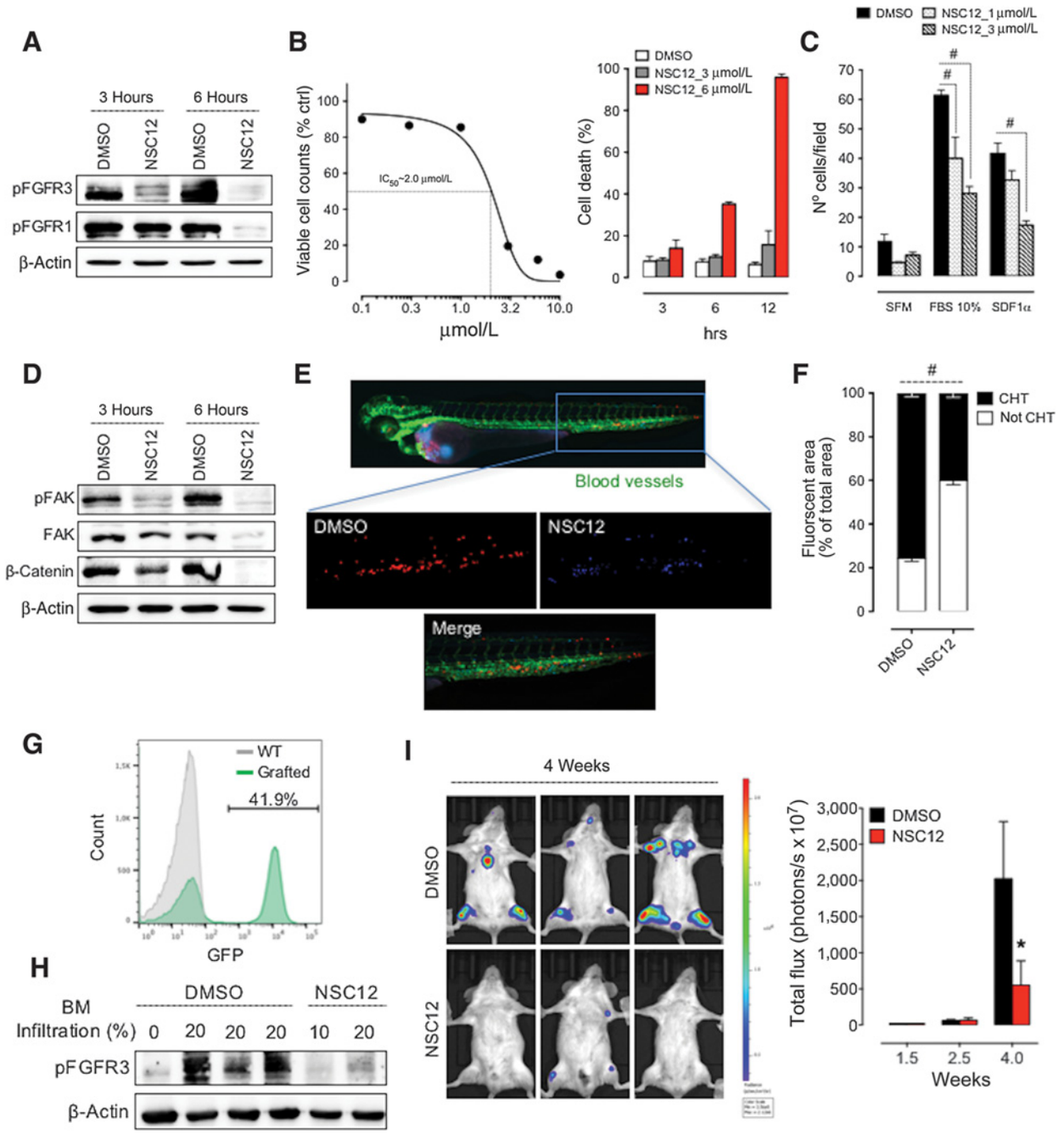

Figure 3.

FGF inhibition hampers MM dissemination. **A,** Western blot analysis of phospho-FGFR1 and phospho-FGFR3 levels in MM.1S cells treated with NSC12 6 μmol/L. **B,** Viable cell counts and apoptotic cell death by cytofluorimetric analysis of NSC12-treated MM.1S cells. **C,** Quantification of MM.1S cells migrated toward chemotactic stimuli in a chemotaxis assay. **D,** Western blot analysis of phospho and total FAK and β-catenin levels in MM.1S cells treated with NSC12 6 μmol/L. **E** and **F,** DMSO- or NSC12-treated MM.1S cells (6 μmol/L for 3 hours) were stained with red or blue fluorescent dye, respectively, injected in the Zebrafish Cuvier Duct and assessed for their ability to migrate to the zebrafish CHT (**E**). Fluorescent area of MM.1S cells inside or outside the CHT were quantified by ImageJ software (**F**). $n = 33$ zebrafish embryos/group. **G,** Cytofluorimetric analysis of BM colonization by GFP/Luciferase-expressing MM.1S 8 weeks after intravenous injection in SCID beige mice. **H,** GFP/Luciferase-expressing MM.1S cells were injected intravenously in SCID beige mice; when 10%–20% of BM disease infiltration was achieved, mice received a 3-day course of oral NSC12 treatment and Western blot analysis of BM lysates after femur flushing was performed. ($n = 3$ mice/group). **I,** SCID beige mice were injected intravenously with GFP/Luciferase-expressing MM.1S cells and treated intraperitoneally every other day for 4 weeks with NSC12 7.5 mg/kg or vehicle ($n = 12$ mice/group). Bioluminescence imaging (left) and quantification (right) of luciferase-expressing MM.1S cells are shown. Data are mean ± SEM. *, $P < 0.05$; #, $P < 0.001$.

Published OnlineFirst February 24, 2020; DOI: 10.1158/0008-5472.CAN-19-2714

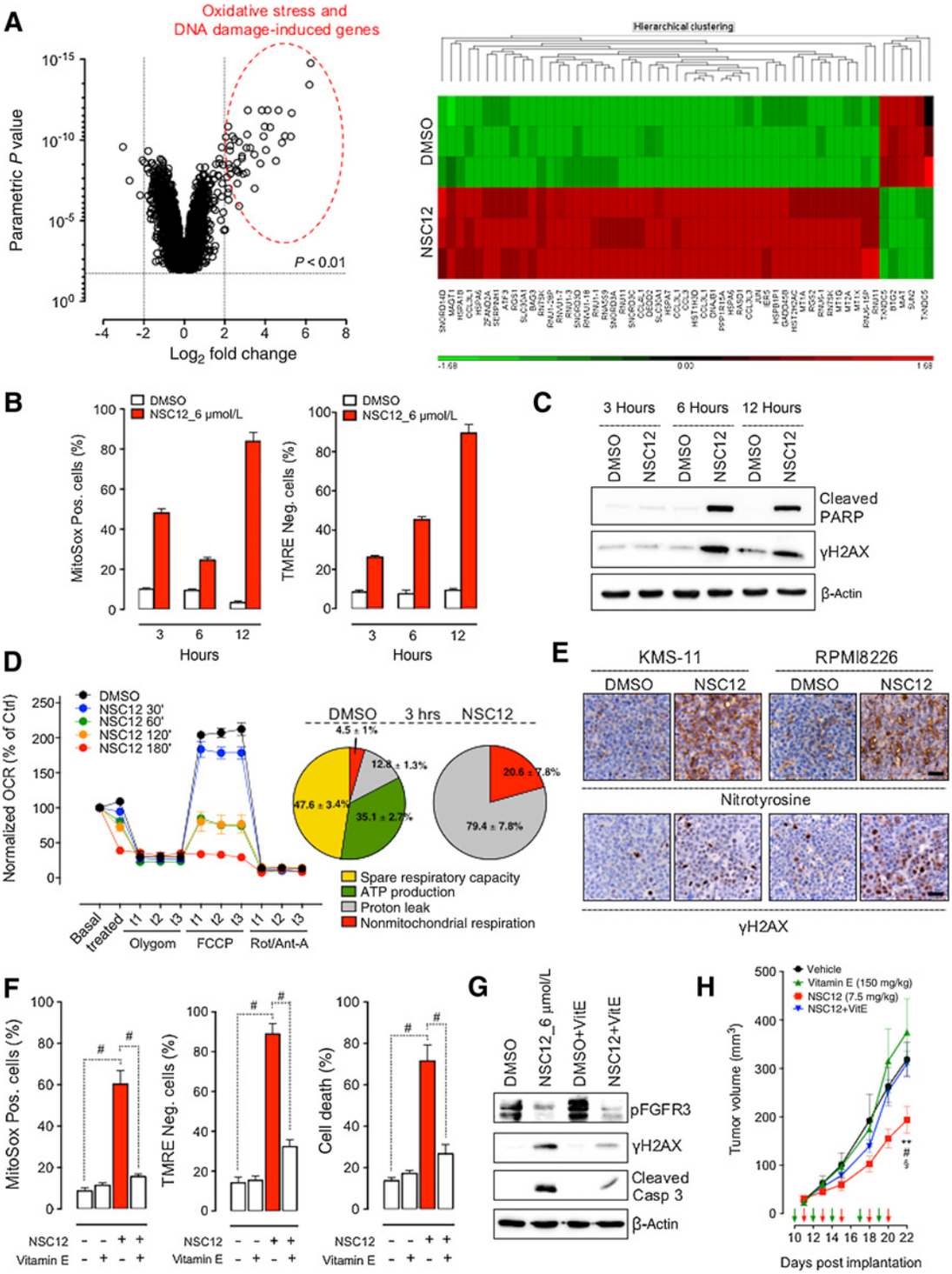

Figure 4.

FGF inhibition induces oxidative stress–mediated apoptosis in MM cells. **A,** Vulcano plot (left) and hierarchical clustering (right) of $\log_2$ two-fold differentially expressed genes ($P < 0.01$) in KMS-11 cells treated with NSC12 6 µmol/L for 12 hours. **B,** Cytofluorimetric analysis of mtROS production (Mitosox) and mitochondrial membrane depolarization (TMRE) in NSC12-treated KMS-11 cells. **C,** Western blot analysis of PARP inactivation and phospho-H2AX (γH2AX) expression in KMS-11 cells treated with NSC12 6 µmol/L. **D,** Analysis of mitochondrial activity by Seahorse assay for OCR in KMS-11 cells treated with NSC12 6 µmol/L. **E,** Anti-nitro tyrosine and anti-pH2AX staining of subcutaneous KMS-11 and RPMI8226 tumors grown in NSC12- or vehicle-treated mice ($n = 5$ mice/group). Scale bar, 50 µm. **F** and **G,** Cytofluorimetric (**F**) and Western blot (**G**) analyses of KMS-11 cells treated with NSC12 6 µmol/L for 12 hours in the presence or absence of vitamin E. Data are mean ± SEM. #, $P < 0.001$. **H,** Tumor growth of KMS-11 cells injected subcutaneously and intraperitoneally treated with NSC12 (red arrows), vitamin E (green arrows), or vehicle ($n = 6$ mice/group).

Published OnlineFirst February 24, 2020; DOI: 10.1158/0008-5472.CAN-19-2714

ptosis in multiple myeloma cells (**Fig. 4F** and **G**; Supplementary Fig. S2G); this occurred without affecting the capacity of the compound to inhibit FGFR phosphorylation (**Fig. 4G**), demonstrating that the rescue effect exerted by vitamin E was due to its antioxidant properties rather than to nonspecific effects interfering with the FGF trap activity of NSC12. Accordingly, *in vivo* vitamin E treatment significantly inhibited the antitumor activity exerted by NSC12 on KMS-11 xenografts (**Fig. 4H**; Supplementary Fig. S3A). Finally, vitamin E exerted a rescue effect also when FGFR signaling was inhibited by the TK FGFR inhibitor BGJ398 (Supplementary Fig. S2G).

In keeping with the hypothesis that FGF inhibition exerts its antitumor activity by inducing mitochondrial oxidative stress, overexpression of mitochondrial catalase (23), but not cytoplasmic catalase, significantly reduced mtROS production and cell death in NSC12-treated KMS-11 cells (Supplementary Fig. S3B) and hampered the antitumor activity of NSC12 *in vivo* (Supplementary Fig. S3C). Together, these data highlight the capacity of the autocrine FGF/FGFR axis to prevent mitochondrial oxidative stress, thus allowing cell survival in multiple myeloma.

c-Myc degradation mediates oxidative stress and apoptosis induced by FGF inhibition in multiple myeloma cells

To understand the mechanism by which the inhibition of FGF signaling triggers oxidative stress–induced cell death in MM, gene set enrichment analysis (GSEA) of GEP data was performed on NSC12-treated KMS-11 cells. In agreement with the impact of FGF inhibition on multiple myeloma cell proliferation/survival and migration, GSEA showed the enrichment of mitotic spindle, G_2–M checkpoint, and Wnt/β-catenin signaling hallmarks that were significantly downmodulated after NSC12 treatment (Supplementary Fig. S4A). GSEA revealed also the downmodulation of c-Myc targets (**Fig. 5A**), confirmed by qRT-PCR (Supplementary Fig. S4B). Accordingly, a rapid disappearance of c-Myc protein occurred in multiple myeloma cells after NSC12 treatment (**Fig. 5B**; Supplementary Fig. S4C) in the absence of significant changes of *c-MYC* mRNA levels at 3 and 6 hours of NSC12 treatment (Supplementary Fig. S4D), suggesting that FGF inhibition may induce proteasomal degradation of c-Myc protein. Indeed, the proteasome inhibitor MG132 prevented c-Myc protein degradation triggered by NSC12 in KMS-11 cells (**Fig. 5C**).

GSK3αβ kinase is a FGFR-mediated modulator of proteasomal c-Myc degradation (32, 37–39). NSC12 inhibited GSK3αβ kinase phosphorylation, leading to the activation of this kinase (**Fig. 5B**; ref. 40). A significant reduction of c-Myc and phospho-GSK3αβ kinase levels was observed also in NSC12-treated KMS-11 tumor xenografts (**Fig. 5B**), suggesting that GSK3αβ kinase activation following FGF trapping may induce c-Myc proteasomal degradation, leading to downregulation of c-Myc target genes.

To assess the role of c-Myc degradation in oxidative stress and apoptosis induced by FGF inhibition in multiple myeloma cells, we generated KMS-11 cells overexpressing the undegradable T58A-mutant form of c-Myc (41, 42). Ectopic expression of the c-Myc$^{(T58A)}$ mutant prevented NSC12-induced c-Myc degradation (**Fig. 5D**) and blocked NSC12-induced production of mtROS, thus preserving multiple myeloma cells from apoptosis (**Fig. 5E**).

The intracellular content of the antioxidant GSH is depleted upon c-Myc downregulation, thus mediating c-Myc–dependent drug-induced apoptosis (43). Accordingly, GSH levels were reduced in NSC12-treated KMS-11 (**Fig. 5F**) and RPMI8226 (Supplementary Fig. S4E) cells, but not in Myc$^{(T58A)}$ KMS-11 cells (**Fig. 5G**). Notably, a reduction of GSH levels in KMS-11 cells significantly occurred as early as 3 hours after NSC12 treatment and return to basal levels at 6 hours. In parallel, ROS production increased 3 hours after treatment to decrease at 6 hours (**Fig. 4B**). In RPMI8226 cells, GSH levels were progressively reduced by increasing the time of exposure to NSC12 (Supplementary Fig. S4E) and, again, GSH depletion was paralleled by ROS production (Supplementary Fig. S2D). These results indicate that ROS production is strictly correlated to GSH depletion in both cell lines and GSH depletion is an early event in NSC12-treated multiple myeloma cells (transiently reversible in KMS11 cells but not in RPMI8226 cells). Accordingly, vitamin E did not significantly prevent GSH depletion in KMS-11 cells upon treatment with NSC12 (**Fig. 5H**).

Altogether, these data suggest that GSH depletion might represent an upstream event in the oxidative stress cascade triggered by c-Myc degradation induced by the inhibition of the autocrine FGF/FGFR system in multiple myeloma cells.

FGF inhibition induces oxidative stress and cell death in newly diagnosed and refractory/relapsed patient-derived multiple myeloma cells

Two clinical trials using selective TK FGFR inhibitors (MyDRUG study: erdafitinib phase I; NCI-MATCH trial: AZD4547 phase II) are ongoing in patients with relapsed/refractory multiple myeloma. On this basis, to assess the therapeutic implications consequent to FGF inhibition in multiple myeloma, tumor cells freshly isolated from 26 multiple myeloma patients (Supplementary Table S2) were treated with NSC12 and assessed for cell death. Twenty-two cases responded to NSC12 regardless of t(4;14) translocation (**Fig. 6A**; Supplementary Table S2). Interestingly, NSC12 was efficacious in both newly diagnosed (10/10) and refractory/relapsed (12/16) patients (Supplementary Table S2). In both cases, Western blot analysis showed a strong inhibition of FGFR3, $ERK_{1/2}$, JAK2, and STAT3 phosphorylation, reduction of mcl-1 levels, and caspase 3 activation (**Fig. 6B**). Only a limited effect, in the absence of caspase-3 activation (Supplementary Fig. S5), was exerted by the highest dose of NSC12 on PBMCs isolated from 8 healthy donors, being totally ineffective at lower doses (**Fig. 6A**).

As observed for multiple myeloma cell lines, NSC12 caused a drastic reduction of c-Myc protein from both newly diagnosed and relapsed/refractory patients (**Fig. 6C**), paralleled by increased oxidative stress and DNA damage, as assessed by qRT-PCR analysis (**Fig. 6D**) and anti-nitro tyrosine and phospho-H2AX staining (**Fig. 6E**). Again, vitamin E rescued patient-derived multiple myeloma cells from NSC12-induced cell death (**Fig. 6F**).

Notably, no significant differences in NSC12 sensitivity were observed between multiple myeloma cells from refractory/relapsed or newly diagnosed patients (**Fig. 7A**). Accordingly, bortezomib-resistant KMS-11/BTZ cells responded *in vitro* and *in vivo* to NSC12 treatment in a manner similar to parental KMS-11 cells (**Fig. 7B**; Supplementary Fig. S6), suggesting that FGF inhibition may represent a therapeutic approach for multiple myeloma cases relapsed from or not responding to proteasome inhibitor-based treatments. In this frame, GEP (Supplementary Table S1) and qRT-PCR (**Fig. 7C**) analyses revealed a significant downregulation of *TXNDC5* and of the c-Myc target *PRDX3* genes in NSC12-treated KMS-11 and KMS-11/BTZ cells (**Fig. 7C**). The two genes are involved in the protection from oxidative stress and bortezomib resistance in refractory/relapsed multiple myeloma (44).

Combined treatment of parental KMS-11 cells with NSC12 plus bortezomib (both administered at their IC_{50} dose) resulted in an additive effect when compared with single treatments and showed a slightly increased efficacy in KMS-11/bortezomib cells (**Fig. 7D**). Accordingly, calculation of the NSC12/bortezomib combination index

Published OnlineFirst February 24, 2020; DOI: 10.1158/0008-5472.CAN-19-2714

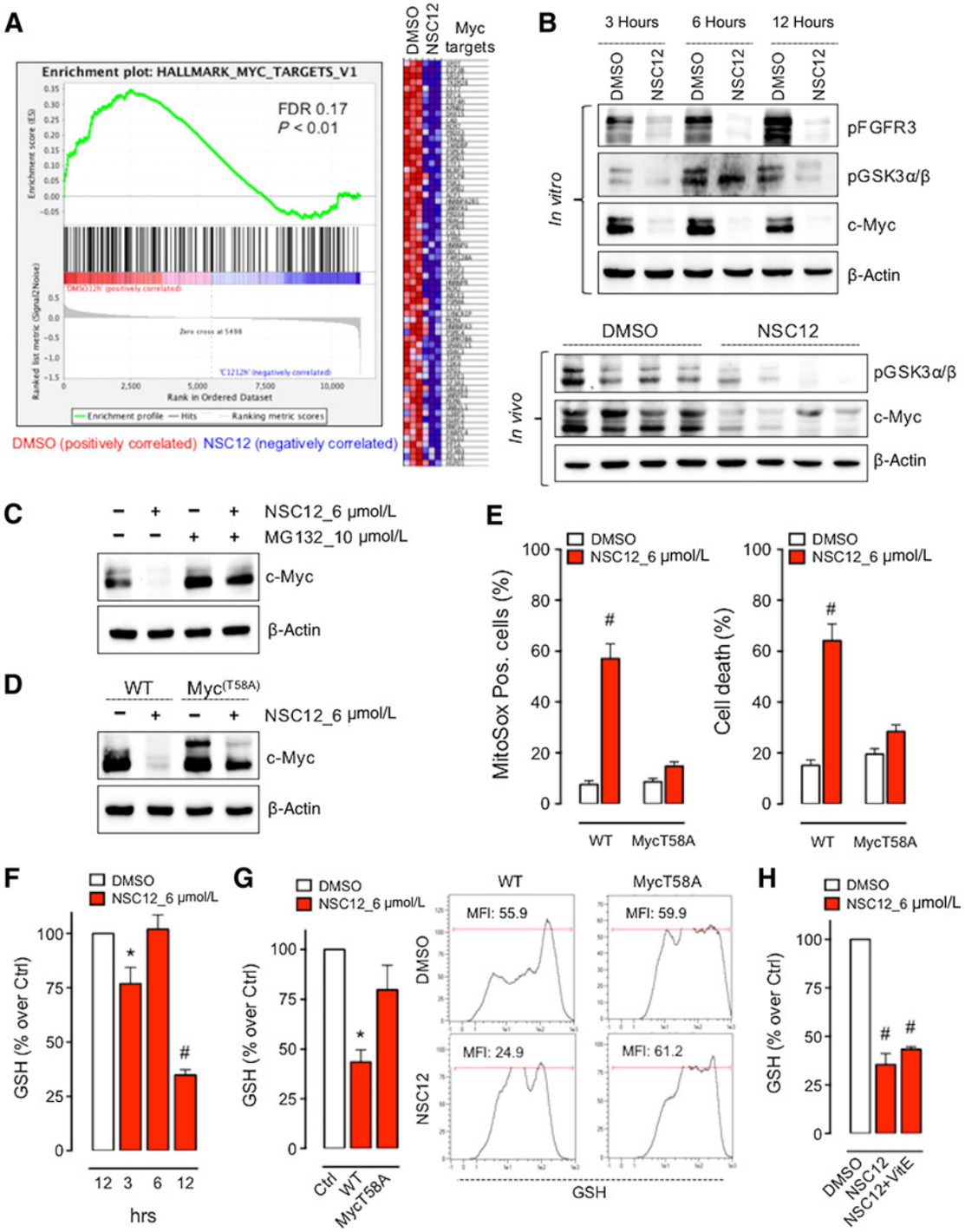

Figure 5.

Oxidative stress–induced apoptosis following FGF inhibition is c-Myc-dependent. **A,** GSEA for c-Myc targets in KMS-11 cells treated with NSC12 6 μmol/L for 12 hours. **B,** Western blot analysis of KMS-11 cells treated with NSC12 6 μmol/L (top) and KMS-11 subcutaneous tumors (bottom) grown in NSC12- or vehicle-treated mice. **C,** Western blot analysis of c-Myc levels in KMS-11 cells treated with NSC12 6 μmol/L for 3 hours in the presence or absence of the proteasome inhibitor MG132. **D,** Western blot analysis of c-Myc levels in WT and Myc$^{(T58A)}$-mutant KMS-11 cells treated with NSC12 6 μmol/L for 3 hours. **E,** Cytofluorimetric analysis of mtROS production and apoptotic cell death in WT and Myc$^{(T58A)}$-mutant KMS-11 cells after 12 hours of NSC12 treatment. **F,** Cytofluorimetric analysis of intracellular GSH content in KMS-11 cells after treatment with NSC12 6 μmol/L. **G,** Cytofluorimetric analysis of intracellular GSH content in WT and Myc$^{(T58A)}$-mutant KMS-11 cells treated with NSC12 6 μmol/L for 12 hours. Values of GSH median fluorescence intensity are reported in the histogram plot. **H,** Cytofluorimetric analysis of intracellular GSH content in KMS-11 cells treated with NSC12 6 μmol/L for 12 hours in the presence or absence of vitamin E. Data are mean ± SEM. *, $P < 0.05$; #, $P < 0.001$.

Published OnlineFirst February 24, 2020; DOI: 10.1158/0008-5472.CAN-19-2714

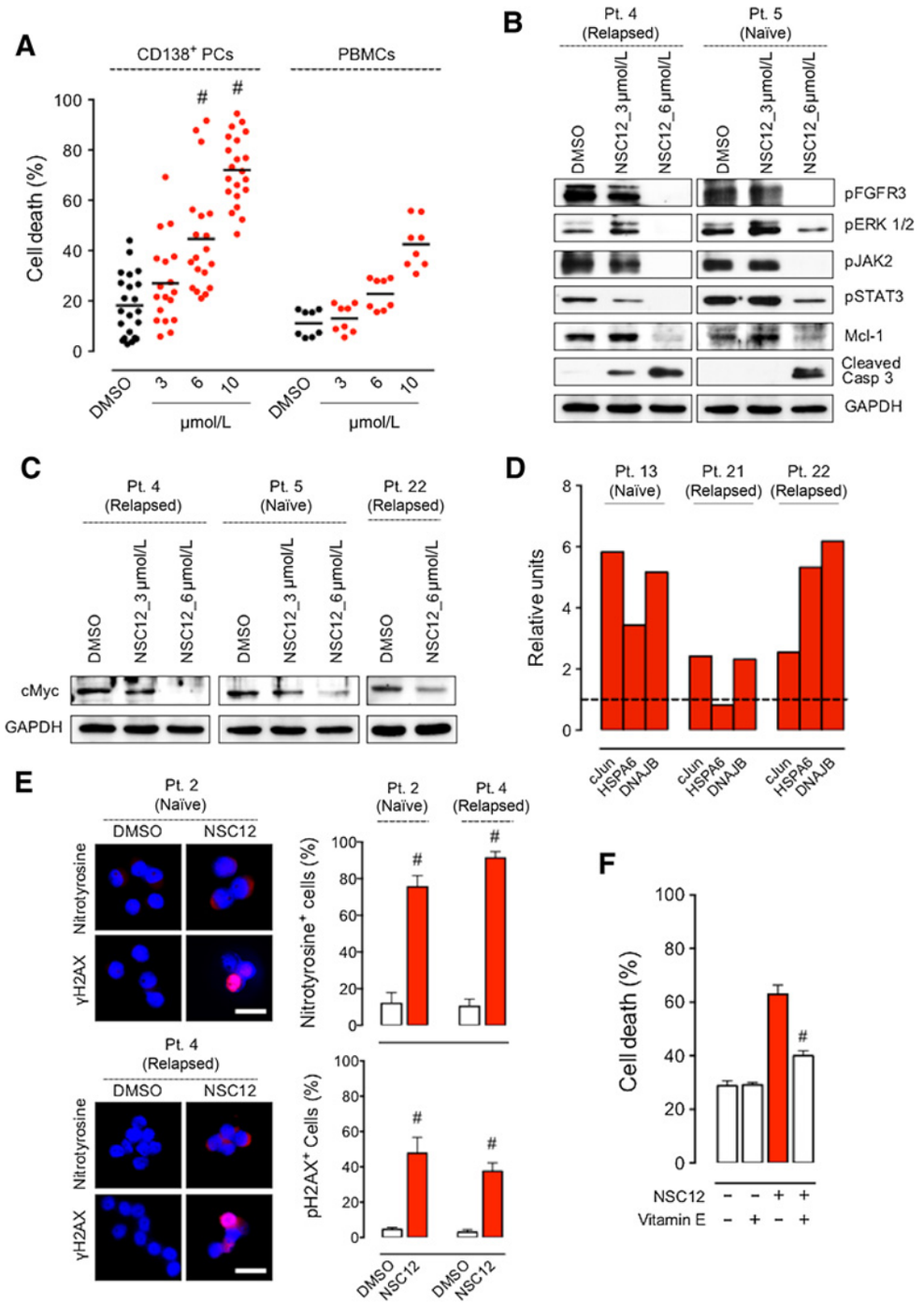

Figure 6.

Effect of FGF trapping in patient-derived multiple myeloma cells. **A,** Analysis of patient-derived multiple myeloma cell death after 12 hours of treatment with increasing doses of NSC12. Only NSC12-responsive multiple myeloma cases are reported (22 cases of 26). PBMCs were tested as control. Each dot represents a single multiple myeloma case or PBMC isolate, and lines indicate the mean values ($n = 26$ multiple myeloma cases; $n = 8$ PBMC isolates). **B** and **C,** Western blot analysis of multiple myeloma cells purified from newly diagnosed (naïve) and relapsed/refractory patients and treated with NSC12 for 12 hours; GAPDH was probed for loading control ($n = 3$ multiple myeloma cases). GAPDH image for patients 4 and 5 are the same in **B** and **C** because they were obtained from the same blot. **D,** qPCR analysis for the expression levels of oxidative stress–induced genes in patient-derived multiple myeloma cells treated with NSC12 6 μmol/L for 6 hours ($n = 3$ multiple myeloma cases). **E,** Immunofluorescence analysis and quantification of patient-derived multiple myeloma cells treated with NSC12 6 μmol/L for 12 hours ($n = 2$ multiple myeloma cases). Scale bar, 20 μm. **F,** Cytofluorimetric analysis of patient-derived multiple myeloma cells treated with NSC12 10 μmol/L for 12 hours in the presence or absence of vitamin E ($n = 3$ multiple myeloma cases). Data are mean ± SEM. #, $P < 0.001$.

Published OnlineFirst February 24, 2020; DOI: 10.1158/0008-5472.CAN-19-2714

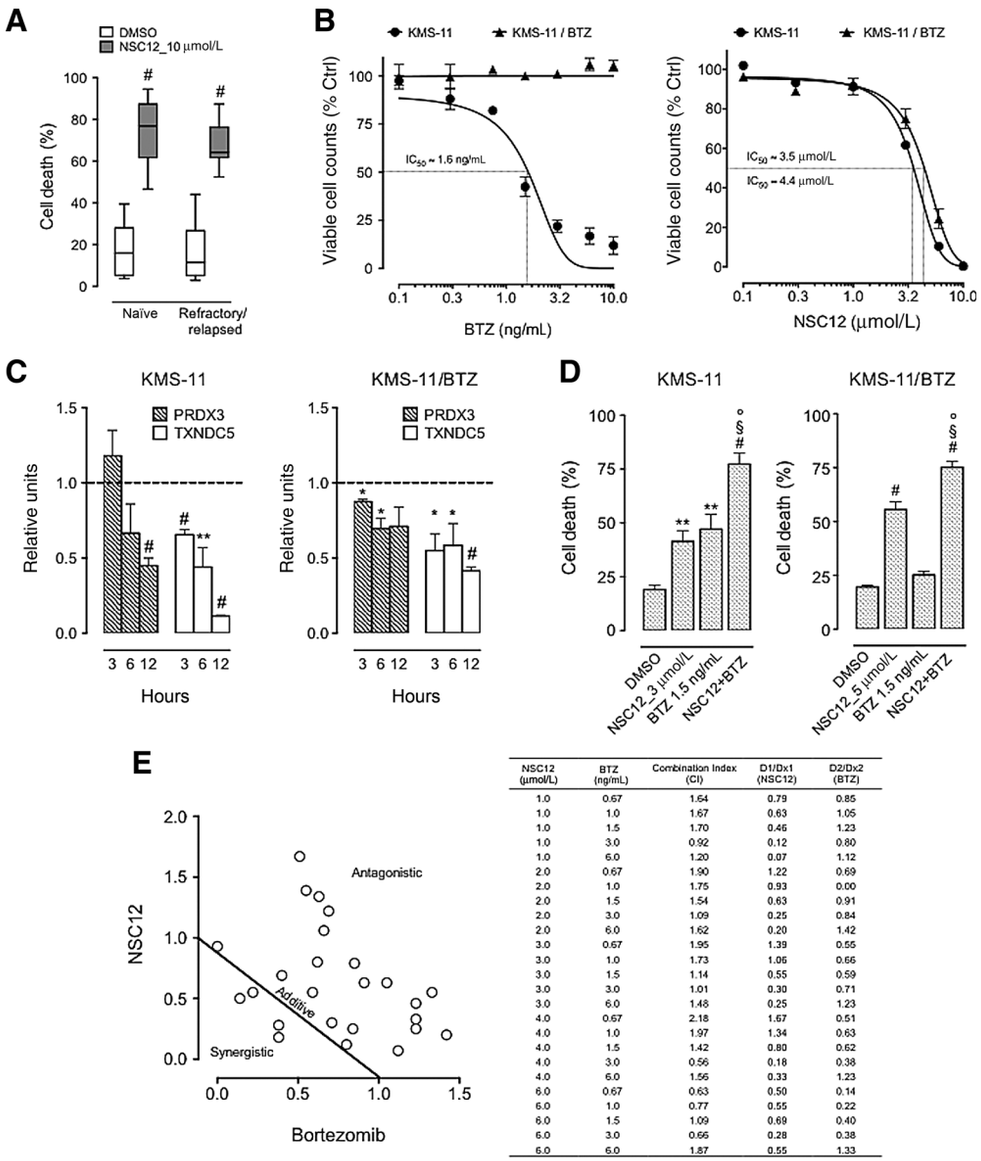

NSC12 (μmol/L)	BTZ (ng/mL)	Combination Index (CI)	D1/Dx1 (NSC12)	D2/Dx2 (BTZ)
1.0	0.67	1.64	0.79	0.85
1.0	1.0	1.67	0.63	1.05
1.0	1.5	1.70	0.46	1.23
1.0	3.0	0.92	0.12	0.80
1.0	6.0	1.20	0.07	1.12
2.0	0.67	1.90	1.22	0.69
2.0	1.0	1.75	0.93	0.00
2.0	1.5	1.54	0.63	0.91
2.0	3.0	1.09	0.25	0.84
2.0	6.0	1.62	0.20	1.42
3.0	0.67	1.95	1.39	0.55
3.0	1.0	1.73	1.06	0.66
3.0	1.5	1.14	0.55	0.59
3.0	3.0	1.01	0.30	0.71
3.0	6.0	1.48	0.25	1.23
4.0	0.67	2.18	1.67	0.51
4.0	1.0	1.97	1.34	0.63
4.0	1.5	1.42	0.80	0.62
4.0	3.0	0.56	0.18	0.38
4.0	6.0	1.56	0.33	1.23
6.0	0.67	0.63	0.50	0.14
6.0	1.0	0.77	0.55	0.22
6.0	1.5	1.09	0.69	0.40
6.0	3.0	0.66	0.28	0.38
6.0	6.0	1.87	0.55	1.33

Figure 7.

Resistance to bortezomib does not affect the antitumor activity of FGF blockade. **A,** Multiple myeloma cells purified from naïve or refractory/relapsed patients were treated with NSC12 10 μmol/L for 12 hours and cell death assessed by cytofluorimetric analysis ($n = 26$ multiple myeloma cases). **B,** Bortezomib-resistant (KMS-11/BTZ) or parental KMS-11 cells were treated with increasing doses of bortezomib or NSC12 for 48 hours and assessed for viable cell counting by cytofluorimetric analysis. **C,** qPCR analysis for the expression levels of *TXNCD5* and *PRDX3* genes in parental and bortezomib-resistant KMS-11 cells treated with NSC12 6 μmol/L. **D,** Cytofluorimetric analysis of apoptotic cell death in KMS-11 and KMS-11/bortezomib cells treated with NSC12 and bortezomib as single agents or in combination. *, $P < 0.05$; **, $P < 0.01$; #, $P < 0.001$ versus DMSO. For KMS-11: §, $P < 0.01$ versus NSC12; °, $P < 0.05$ versus bortezomib; for KMS-11/BTZ: §, $P < 0.01$ versus NSC12; °, $P < 0.001$ versus bortezomib. **E,** Left, normalized isobologram for nonconstant ratio combinations. The normalized doses are given on the *y*- and *x*-axis for NSC12 (D_1/Dx_1) and bortezomib (D_2/Dx_2), respectively. Combination data points falling on the diagonal indicate additive effect; data points falling in the lower left or upper right quadrants of the diagonal indicate synergism or antagonism, respectively. Right, value of combination index for NSC12 (1–6 μmol/L) and bortezomib (0.67–6 ng/mL) used in a nonconstant ratio. Data are mean ± SEM. In box and whisker graphs, boxes extend from the 25th to the 75th percentiles, lines indicate the median values, and whiskers indicate the range of values. *, $P < 0.05$; **, $P < 0.01$; #, $P < 0.001$.

showed additive effects on KMS-11 cells limited to few doses of the two compounds, the majority of them producing antagonistic effects (**Fig. 7E**), possibly related to the capacity of high doses of bortezomib to prevent c-Myc degradation triggered by NSC12 treatment (Supplementary Fig. S7). This is in keeping with our data showing that proteasome inhibition by MG132 abrogates NSC12-induced c-Myc degradation (**Fig. 5C**), which, in turn, is essential to induce multiple myeloma cell death.

Altogether, these findings indicate that FGF/FGFR inhibitors may represent a promising approach to eradicate bortezomib-refractory multiple myeloma cells but raise possible concerns about their use in combination with proteasome inhibitors.

Published OnlineFirst February 24, 2020; DOI: 10.1158/0008-5472.CAN-19-2714

Discussion

Here we show for the first time that the autocrine FGF/FGFR-dependent signaling protects multiple myeloma cells from oxidative stress–induced apoptosis, thus playing a nonredundant role in multiple myeloma cell survival. Indeed, we demonstrate that FGF blockade induces the degradation of the oncoprotein c-Myc; this causes GSH depletion and triggers mitochondrial oxidative stress, DNA damage, and apoptosis in multiple myeloma cells.

In keeping with data obtained using the FGFR kinase inhibitor BGJ398 in FGFR1 fusion-driven hematologic malignancies (45), here we observed a significant downmodulation of c-Myc targets after FGF inhibition in multiple myeloma cells. Accordingly, FGF blockade induced the degradation of c-Myc protein that was inhibited by the proteasome inhibitor MG132. This was paralleled by activation of GSK3αβ kinase, a direct regulator of c-Myc degradation (37, 38). In addition, ectopic expression of the undegradable c-Myc$^{(T58A)}$-mutant (41) prevented NSC12-induced mtROS production and apoptosis in KMS-11 cells. Together, these findings point to a direct link between FGF signaling, c-Myc activity, and cell survival in multiple myeloma.

c-Myc controls mitochondrial metabolism and homeostasis (46) and upregulates the levels of mitochondrial glutaminase, leading to GSH synthesis (47). In turn, GSH prevents apoptosis due to ROS production consequent to redox imbalance or enhanced mitochondrial function in response to increased c-Myc activity (48, 49). In keeping with these findings, recent evidences show that primary multiple myeloma cells may depend on c-Myc activity for survival (50, 51). Accordingly, upregulation of c-Myc protein is related to multiple myeloma disease initiation and progression, being activated in a large fraction of multiple myeloma patients (52–54). Our data show that FGF trapping causes a significant depletion of GSH levels in wild-type KMS-11 cells but not in Myc$^{(T58A)}$ mutants, thus indicating that FGF/FGFR signaling protects multiple myeloma cells from oxidative stress–mediated apoptosis through c-Myc-dependent regulation of GSH levels.

Oxidative stress–inducing agents have been approved for the treatment of solid malignancies and various types of leukemias and lymphomas (55). Several evidences suggest that affecting the intracellular redox status may represent a promising strategy also in multiple myeloma. Indeed, elevated serum levels of oxidative stress markers are found in patients with multiple myeloma (56, 57). In addition, upregulation of the antioxidant superoxide dismutase-1 and epigenetic silencing of the oxidative stress sensitizer GSH peroxidase 3 gene are associated to multiple myeloma progression and poor prognosis (58, 59). Also, the small nucleolar RNA ACA11 inhibits oxidative stress and is overexpressed in patient-derived t(4;14)-positive multiple myeloma cells (60). Altogether, these evidences indicate that the induction of ROS production by FGF/FGFR inhibitors may represent a novel anti-multiple myeloma approach. Moreover, our experimental data aimed at reducing mitochondrial oxidative stress via vitamin E administration and mitochondrial catalase overexpression suggest that the use of antioxidant supplements (61) in the context of FGF/FGFR inhibitory therapies should be carefully evaluated.

Our findings were confirmed within the clinical setting using primary BM-derived plasma cells from multiple myeloma patients. Twenty-two out of the 26 examined cases responded significantly to the NSC12-mediated FGF trapping approach regardless of the presence of the t(4;14) chromosomal translocation. This is in keeping with the fact that the vast majority of multiple myeloma tumors harboring this chromosomal translocation show an upregulated expression of the wild-type FGFR3 receptor that still depends on FGF ligand(s) for activation (17). Thus, FGF inhibition might represent a promising therapeutic strategy in multiple myeloma, including high-risk multiple myeloma patients with the t(4;14) translocation.

Notably, NSC12 reduced the levels of c-Myc protein and increased oxidative stress also in multiple myeloma primary cells obtained from patients with relapsed/refractory disease. Accordingly, NSC12 treatment exerts a similar oncosuppressive effect on both parental and bortezomib-resistant (KMS-11/BTZ) KMS-11 cells *in vitro* and *in vivo*. This goes in parallel with the inhibition of the expression of *TXNDC5* and of the c-Myc target *PRDX3*, both involved in the protection from mitochondrial oxidative stress and bortezomib resistance in refractory/relapsed multiple myeloma (44). In this context, our data indicate that proteasome inhibition can substantially abrogate the effect exerted by FGF blockade on c-Myc degradation, which, in turn, is essential to induce multiple myeloma cell death. Thus, even though previous observations have shown that perturbation of mitochondrial function may decrease the resistance of multiple myeloma cells to bortezomib (62), therapies based on the combination of FGF/FGFR and proteasome inhibitors may show a limited therapeutic window.

Four out of the 26 patient-derived multiple myeloma cell cases tested showed a limited or no response to FGF inhibition. Our data point to c-Myc as a key downstream effector able to determine the therapeutic response to FGF/FGFR inhibitors in multiple myeloma. Even though the presence of point mutations encoding for undegradable forms of c-Myc has not been reported for multiple myeloma (54), recent observations have shown that PKC-dependent phosphorylation of GSK3αβ kinase causes its inactivation in gastric cancer (39), thus representing a possible mechanism of resistance/escape to anti-FGF therapies. Further studies will be required to get a deeper insight into the molecular mechanisms that allow or hamper the response to therapeutic approaches targeting the FGF/FGFR system in multiple myeloma.

To the best of our knowledge, two clinical trials using selective TK FGFR inhibitors (MyDRUG study: Erdafitinib; NCI-MATCH trial: AZD4547) are ongoing in patients with relapsed/refractory multiple myeloma. Rather than representing a possible supportive therapy in combination with proteasome inhibitors, our findings indicate that FGF/FGFR blockade may set the basis for the development of promising second-/third-line approaches to eradicate proteasome inhibitor–relapsed/refractory multiple myeloma cells. Our data together with the results of the ongoing clinical trials will provide helpful information about the efficacy of anti-FGF/FGFR approaches in multiple myeloma therapy.

Disclosure of Potential Conflicts of Interest

No potential conflicts of interest were disclosed.

Authors' Contributions

Conception and design: R. Ronca, M. Mor, M. Presta, A. Giacomini
Development of methodology: E. Foglio, V. Desantis
Acquisition of data (provided animals, acquired and managed patients, provided facilities, etc.): R. Ronca, G.C. Ghedini, F. Maccarinelli, S. L. Locatelli, S. Taranto, E. Grillo, S. Matarazzo, R. Castelli, G. Paganini, N. Cattane, A. Cattaneo, C. Carlo-Stella, A. Belotti, A. Giacomini
Analysis and interpretation of data (e.g., statistical analysis, biostatistics, computational analysis): R. Ronca, E. Grillo, G. Paganini, N. Cattane, A. Cattaneo, A. Giacomini

Writing, review, and/or revision of the manuscript: R. Ronca, R. Castelli, A.M. Roccaro, M. Presta, A. Giacomini
Administrative, technical, or material support (i.e., reporting or organizing data, constructing databases): G.C. Ghedini, S. Taranto
Study supervision: M. Presta, A. Giacomini
Other (isolated patient- derived MM cells and performed *in vitro* experiments): A. Sacco
Other (conceived NSC12 and supervised synthesis): M. Mor
Other (provided primary samples): A.M. Roccaro

Acknowledgments

This work was supported by grants from Fondazione Cariplo (grant no. 2016-0570 to A. Giacomini), Fondazione Regionale per la Ricerca Biomedica (FRRB, grant no. 2016-065 ERA-NET TRANSCAN-2 to A.M. Roccaro) and (FRRB, grant no. 2015-0042 to C. Carlo-Stella) and Associazione Italiana Ricerca sul Cancro (AIRC grant no. 18943 to M. Presta), (AIRC grant no. MFAG 18459 to R. Ronca) and (AIRC grant no. 20575 to C. Carlo-Stella). E. Grillo and S. Matarazzo were supported by Fondazione Italiana per la Ricerca sul Cancro Fellowships and F. Maccarinelli, by a Fondazione Veronesi Fellowship. The authors are grateful to Dr. Daniela Uberti and Dr. Mattia Bugatti for technical support.

The costs of publication of this article were defrayed in part by the payment of page charges. This article must therefore be hereby marked *advertisement* in accordance with 18 U.S.C. Section 1734 solely to indicate this fact.

Received August 29, 2019; revised December 10, 2019; accepted February 14, 2020; published first February 24, 2020.

References

1. Siegel R, Naishadham D, Jemal A. Cancer statistics, 2013. CA Cancer J Clin 2013; 63:11–30.
2. Raab MS, Podar K, Breitkreutz I, Richardson PG, Anderson KC. Multiple myeloma. Lancet 2009;374:324–39.
3. Bommert K, Bargou RC, Stuhmer T. Signalling and survival pathways in multiple myeloma. Eur J Cancer 2006;42:1574–80.
4. van de Donk NW, Lokhorst HM, Bloem AC. Growth factors and antiapoptotic signaling pathways in multiple myeloma. Leukemia 2005;19:2177–85.
5. Ria R, Reale A, De Luisi A, Ferrucci A, Moschetta M, Vacca A. Bone marrow angiogenesis and progression in multiple myeloma. Am J Blood Res 2011; 1:76–89.
6. Ribatti D, Vacca A. New insights in anti-angiogenesis in multiple myeloma. Int J Mol Sci 2018;19:2031. DOI: 10.3390/ijms19072031.
7. Bisping G, Leo R, Wenning D, Dankbar B, Padro T, Kropff M, et al. Paracrine interactions of basic fibroblast growth factor and interleukin-6 in multiple myeloma. Blood 2003;101:2775–83.
8. Lentzsch S, Chatterjee M, Gries M, Bommert K, Gollasch H, Dorken B, et al. PI3-K/AKT/FKHR and MAPK signaling cascades are redundantly stimulated by a variety of cytokines and contribute independently to proliferation and survival of multiple myeloma cells. Leukemia 2004;18:1883–90.
9. Otsuki T, Yamada O, Yata K, Sakaguchi H, Kurebayashi J, Nakazawa N, et al. Expression of fibroblast growth factor and FGF-receptor family genes in human myeloma cells, including lines possessing t(4;14)(q16.3;q32. 3) and FGFR3 translocation. Int J Oncol 1999;15:1205–12.
10. Sato N, Hattori Y, Wenlin D, Yamada T, Kamata T, Kakimoto T, et al. Elevated level of plasma basic fibroblast growth factor in multiple myeloma correlates with increased disease activity. Jpn J Cancer Res 2002;93:459–66.
11. Sezer O, Jakob C, Eucker J, Niemoller K, Gatz F, Wernecke K, et al. Serum levels of the angiogenic cytokines basic fibroblast growth factor (bFGF), vascular endothelial growth factor (VEGF) and hepatocyte growth factor (HGF) in multiple myeloma. Eur J Haematol 2001;66:83–8.
12. Walsh S, Jefferiss C, Stewart K, Jordan GR, Screen J, Beresford JN. Expression of the developmental markers STRO-1 and alkaline phosphatase in cultures of human marrow stromal cells: regulation by fibroblast growth factor (FGF)-2 and relationship to the expression of FGF receptors 1–4. Bone 2000;27:185–95.
13. Plowright EE, Li Z, Bergsagel PL, Chesi M, Barber DL, Branch DR, et al. Ectopic expression of fibroblast growth factor receptor 3 promotes myeloma cell proliferation and prevents apoptosis. Blood 2000;95:992–8.
14. Grand EK, Chase AJ, Heath C, Rahemtulla A, Cross NC. Targeting FGFR3 in multiple myeloma: inhibition of t(4;14)-positive cells by SU5402 and PD173074. Leukemia 2004;18:962–6.
15. Trudel S, Ely S, Farooqi Y, Affer M, Robbiani DF, Chesi M, et al. Inhibition of fibroblast growth factor receptor 3 induces differentiation and apoptosis in t (4;14) myeloma. Blood 2004;103:3521–8.
16. Kalff A, Spencer A. The t(4;14) translocation and FGFR3 overexpression in multiple myeloma: prognostic implications and current clinical strategies. Blood Cancer J 2012;2:e89.
17. Intini D, Baldini L, Fabris S, Lombardi L, Ciceri G, Maiolo AT, et al. Analysis of FGFR3 gene mutations in multiple myeloma patients with t(4;14). Br J Haematol 2001;114:362–4.
18. Krejci P, Mekikian PB, Wilcox WR. The fibroblast growth factors in multiple myeloma. Leukemia 2006;20:1165–8.
19. Giacomini A, Chiodelli P, Matarazzo S, Rusnati M, Presta M, Ronca R. Blocking the FGF/FGFR system as a "two-compartment" antiangiogenic/antitumor approach in cancer therapy. Pharmacol Res 2016;107:172–85.
20. Castelli R, Giacomini A, Anselmi M, Bozza N, Vacondio F, Rivara S, et al. Synthesis, structural elucidation, and biological evaluation of NSC12, an orally available fibroblast growth factor (FGF) ligand trap for the treatment of FGF-dependent lung tumors. J Med Chem 2016;59:4651–63.
21. Ronca R, Giacomini A, Di Salle E, Coltrini D, Pagano K, Ragona L, et al. Long-pentraxin 3 derivative as a small-molecule FGF trap for cancer therapy. Cancer Cell 2015;28:225–39.
22. Bono F, De Smet F, Herbert C, De Bock K, Georgiadou M, Fons P, et al. Inhibition of tumor angiogenesis and growth by a small-molecule multi-FGF receptor blocker with allosteric properties. Cancer Cell 2013;23:477–88.
23. Gurgul E, Lortz S, Tiedge M, Jorns A, Lenzen S. Mitochondrial catalase over-expression protects insulin-producing cells against toxicity of reactive oxygen species and proinflammatory cytokines. Diabetes 2004;53:2271–80.
24. Sacco A, Roccaro AM, Ma D, Shi J, Mishima Y, Moschetta M, et al. Cancer cell dissemination and homing to the bone marrow in a Zebrafish model. Cancer Res 2016;76:463–71.
25. Roccaro AM, Mishima Y, Sacco A, Moschetta M, Tai YT, Shi J, et al. CXCR4 regulates extra-medullary myeloma through epithelial-mesenchymal-transition-like transcriptional activation. Cell Rep 2015;12:622–35.
26. Beenken A, Mohammadi M. The FGF family: biology, pathophysiology and therapy. Nat Rev Drug Discov 2009;8:235–53.
27. Ishikawa H, Tsuyama N, Liu S, Abroun S, Li FJ, Otsuyama K, et al. Accelerated proliferation of myeloma cells by interleukin-6 cooperating with fibroblast growth factor receptor 3-mediated signals. Oncogene 2005;24: 6328–32.
28. Wuillème-Toumi S, Robillard N, Gomez P, Moreau P, Le Gouill S, Avet-Loiseau H, et al. Mcl-1 is overexpressed in multiple myeloma and associated with relapse and shorter survival. Leukemia 2005;19:1248–52.
29. van de Donk NWC J, Lokhorst HM, Bloem AC. Growth factors and antiapoptotic signaling pathways in multiple myeloma. Leukemia 2005;19: 2177–85.
30. Greenstein S, Krett NL, Kurosawa Y, Ma C, Chauhan D, Hideshima T, et al. Characterization of the MM.1 human multiple myeloma (MM) cell lines: a model system to elucidate the characteristics, behavior, and signaling of steroid-sensitive and -resistant MM cells. Exp Hematol 2003;31:271–82.
31. Lwin ST, Edwards CM, Silbermann R. Preclinical animal models of multiple myeloma. BoneKEy Rep 2016;5:772.
32. Hashimoto M, Sagara Y, Langford D, Everall IP, Mallory M, Everson A, et al. Fibroblast growth factor 1 regulates signaling via the glycogen synthase kinase-3beta pathway. Implications for neuroprotection. J Biol Chem 2002;277: 32985–91.
33. Hunger-Glaser I, Fan RS, Perez-Salazar E, Rozengurt E. PDGF and FGF induce focal adhesion kinase (FAK) phosphorylation at Ser-910: dissociation from Tyr-397 phosphorylation and requirement for ERK activation. J Cell Physiol 2004; 200:213–22.
34. Katoh M, Katoh M. Cross-talk of WNT and FGF signaling pathways at GSK3beta to regulate beta-catenin and SNAIL signaling cascades. Cancer Biol Ther 2006;5: 1059–64.
35. Qiang YW, Walsh K, Yao L, Kedei N, Blumberg PM, Rubin JS, et al. Wnts induce migration and invasion of myeloma plasma cells. Blood 2005;106:1786–93.

Published OnlineFirst February 24, 2020; DOI: 10.1158/0008-5472.CAN-19-2714

36. Park SY, Wolfram P, Canty K, Harley B, Nombela-Arrieta C, Pivarnik G, et al. Focal adhesion kinase regulates the localization and retention of pro-B cells in bone marrow microenvironments. J Immunol 2013;190:1094–102.
37. Robertson H, Hayes JD, Sutherland C. A partnership with the proteasome; the destructive nature of GSK3. Biochem Pharmacol 2018;147:77–92.
38. Welcker M, Orian A, Jin J, Grim JE, Harper JW, Eisenman RN, et al. The Fbw7 tumor suppressor regulates glycogen synthase kinase 3 phosphorylation-dependent c-Myc protein degradation. Proc Natl Acad Sci U S A 2004;101: 9085–90.
39. Lau WM, Teng E, Huang KK, Tan JW, Das K, Zang Z, et al. Acquired resistance to FGFR inhibitor in diffuse-type gastric cancer through an AKT-independent PKC-mediated phosphorylation of GSK3beta. Mol Cancer Ther 2018;17:232–42.
40. Fang X, Yu SX, Lu Y, Bast RC Jr, Woodgett JR, Mills GB. Phosphorylation and inactivation of glycogen synthase kinase 3 by protein kinase A. Proc Natl Acad Sci U S A 2000;97:11960–5.
41. Liu H, Ai J, Shen A, Chen Y, Wang X, Peng X, et al. c-Myc alteration determines the therapeutic response to FGFR inhibitors. Clin Cancer Res 2017;23:974–84.
42. Sears RC. The life cycle of C-myc: from synthesis to degradation. Cell Cycle 2004; 3:1133–7.
43. Biroccio A, Benassi B, Fiorentino F, Zupi G. Glutathione depletion induced by c-Myc downregulation triggers apoptosis on treatment with alkylating agents. Neoplasia 2004;6:195–206.
44. Dytfeld D, Luczak M, Wrobel T, Usnarska-Zubkiewicz L, Brzezniakiewicz K, Jamroziak K, et al. Comparative proteomic profiling of refractory/relapsed multiple myeloma reveals biomarkers involved in resistance to bortezomib-based therapy. Oncotarget 2016;7:56726–36.
45. Hu T, Wu Q, Chong Y, Qin H, Poole CJ, van Riggelen J, et al. FGFR1 fusion kinase regulation of MYC expression drives development of stem cell leukemia/lymphoma syndrome. Leukemia 2018;32:2363–73.
46. Chen H, Liu H, Qing G. Targeting oncogenic Myc as a strategy for cancer treatment. Signal Transduct Target Ther 2018;3:5.
47. Gao P, Tchernyshyov I, Chang TC, Lee YS, Kita K, Ochi T, et al. c-Myc suppression of miR-23a/b enhances mitochondrial glutaminase expression and glutamine metabolism. Nature 2009;458:762–5.
48. Bansal A, Simon MC. Glutathione metabolism in cancer progression and treatment resistance. J Cell Biol 2018;217:2291–8.
49. Yuneva M, Zamboni N, Oefner P, Sachidanandam R, Lazebnik Y. Deficiency in glutamine but not glucose induces MYC-dependent apoptosis in human cells. J Cell Biol 2007;178:93–105.
50. Holien T, Vatsveen TK, Hella H, Waage A, Sundan A. Addiction to c-MYC in multiple myeloma. Blood 2012;120:2450–3.
51. Shaffer AL, Emre NC, Lamy L, Ngo VN, Wright G, Xiao W, et al. IRF4 addiction in multiple myeloma. Nature 2008;454:226–31.
52. Chng WJ, Huang GF, Chung TH, Ng SB, Gonzalez-Paz N, Troska-Price T, et al. Clinical and biological implications of MYC activation: a common difference between MGUS and newly diagnosed multiple myeloma. Leukemia 2011;25: 1026–35.
53. Cobbold LC, Wilson LA, Sawicka K, King HA, Kondrashov AV, Spriggs KA, et al. Upregulated c-myc expression in multiple myeloma by internal ribosome entry results from increased interactions with and expression of PTB-1 and YB-1. Oncogene 2010;29:2884–91.
54. Dib A, Gabrea A, Glebov OK, Bergsagel PL, Kuehl WM. Characterization of MYC translocations in multiple myeloma cell lines. J Natl Cancer Inst Monogr 2008:25–31.
55. Gorrini C, Harris IS, Mak TW. Modulation of oxidative stress as an anticancer strategy. Nat Rev Drug Discov 2013;12:931–47.
56. Gangemi S, Allegra A, Alonci A, Cristani M, Russo S, Speciale A, et al. Increase of novel biomarkers for oxidative stress in patients with plasma cell disorders and in multiple myeloma patients with bone lesions. Inflamm Res 2012;61:1063–7.
57. Mehdi WA, Zainulabdeen JA, Mehde AA. Investigation of the antioxidant status in multiple myeloma patients: effects of therapy. Asian Pac J Cancer Prev 2013; 14:3663–7.
58. Kaiser MF, Johnson DC, Wu P, Walker BA, Brioli A, Mirabella F, et al. Global methylation analysis identifies prognostically important epigenetically inactivated tumor suppressor genes in multiple myeloma. Blood 2013;122: 219–26.
59. Salem K, McCormick ML, Wendlandt E, Zhan F, Goel A. Copper-zinc superoxide dismutase-mediated redox regulation of bortezomib resistance in multiple myeloma. Redox Biol 2015;4:23–33.
60. Chu L, Su MY, Maggi LB Jr, Lu L, Mullins C, Crosby S, et al. Multiple myeloma-associated chromosomal translocation activates orphan snoRNA ACA11 to suppress oxidative stress. J Clin Invest 2012;122:2793–806.
61. Moss RW. Should patients undergoing chemotherapy and radiotherapy be prescribed antioxidants? Integr Cancer Ther 2006;5:63–82.
62. Song IS, Kim HK, Lee SR, Jeong SH, Kim N, Ko KS, et al. Mitochondrial modulation decreases the bortezomib-resistance in multiple myeloma cells. Int J Cancer 2013;133:1357–67.

Published OnlineFirst February 24, 2020; DOI: 10.1158/0008-5472.CAN-19-2714

Cancer Research
The Journal of Cancer Research (1916–1930) | The American Journal of Cancer (1931–1940)

AACR American Association for Cancer Research

FGF Trapping Inhibits Multiple Myeloma Growth through c-Myc Degradation–Induced Mitochondrial Oxidative Stress

Roberto Ronca, Gaia C. Ghedini, Federica Maccarinelli, et al.

Cancer Res 2020;80:2340-2354. Published OnlineFirst February 24, 2020.